



Kent Academic Repository

Hale, John, An, Xiuli, Guo, Xinhua, Gao, Erjing, Papoin, Julien, Blanc, Lionel, Hillyer, Christopher D., Gratzner, Walter, Baines, Anthony and Mohandas, Narla (2021) *I-spectrin represents evolutionary optimization of spectrin for red blood cell deformability*. *Biophysical Journal* . ISSN 0006-3495.

Downloaded from

<https://kar.kent.ac.uk/89641/> The University of Kent's Academic Repository KAR

The version of record is available from

<https://doi.org/10.1016/j.bpj.2021.07.027>

This document version

Publisher pdf

DOI for this version

Licence for this version

CC BY-NC-ND (Attribution-NonCommercial-NoDerivatives)

Additional information

Versions of research works

Versions of Record

If this version is the version of record, it is the same as the published version available on the publisher's web site. Cite as the published version.

Author Accepted Manuscripts

If this document is identified as the Author Accepted Manuscript it is the version after peer review but before type setting, copy editing or publisher branding. Cite as Surname, Initial. (Year) 'Title of article'. To be published in *Title of Journal* , Volume and issue numbers [peer-reviewed accepted version]. Available at: DOI or URL (Accessed: date).

Enquiries

If you have questions about this document contact ResearchSupport@kent.ac.uk. Please include the URL of the record in KAR. If you believe that your, or a third party's rights have been compromised through this document please see our [Take Down policy](https://www.kent.ac.uk/guides/kar-the-kent-academic-repository#policies) (available from <https://www.kent.ac.uk/guides/kar-the-kent-academic-repository#policies>).

Journal Pre-proof

α -spectrin represents evolutionary optimization of spectrin for red blood cell deformability.

John Hale, Xiuli An, Xinhua Guo, Erjing Gao, Julien Papoin, Lionel Blanc, Christopher D. Hillyer, Walter Gratzer, Anthony Baines, Narla Mohandas

PII: S0006-3495(21)00637-8

DOI: <https://doi.org/10.1016/j.bpj.2021.07.027>

Reference: BPJ 11233

To appear in: *Biophysical Journal*

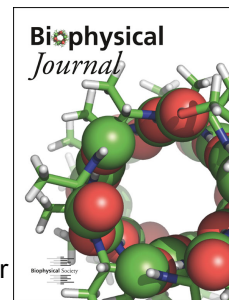
Received Date: 22 March 2021

Accepted Date: 28 July 2021

Please cite this article as: Hale J, An X, Guo X, Gao E, Papoin J, Blanc L, Hillyer CD, Gratzer W, Baines A, Mohandas N, α -spectrin represents evolutionary optimization of spectrin for red blood cell deformability., *Biophysical Journal* (2021), doi: <https://doi.org/10.1016/j.bpj.2021.07.027>.

This is a PDF file of an article that has undergone enhancements after acceptance, such as the addition of a cover page and metadata, and formatting for readability, but it is not yet the definitive version of record. This version will undergo additional copyediting, typesetting and review before it is published in its final form, but we are providing this version to give early visibility of the article. Please note that, during the production process, errors may be discovered which could affect the content, and all legal disclaimers that apply to the journal pertain.

© 2021 Biophysical Society.



α -spectrin represents evolutionary optimization of spectrin for red blood cell deformability.

Running title: α -spectrin key to RBC deformability

Authors

John Hale^{1*}, Xiuli An², Xinhua Guo², Erjing Gao¹, Julien Papoin³, Lionel Blanc^{3,4}, Christopher D. Hillyer¹, Walter Gratzer⁵, Anthony Baines⁶ and Narla Mohandas¹

Affiliations

1 The Red Cell Physiology Laboratory, The New York Blood Center, New York, New York 10021

2 Membrane Biology Laboratory, The New York Blood Center, New York, New York 10021

3 Nelkin Laboratory of Pediatric Oncology and Laboratory of Developmental Erythropoiesis, The Feinstein Institutes for Medical Research, Manhasset, NY 11030

4 Department of Molecular Medicine and Pediatrics, Zucker School of Medicine at Hofstra/Northwell, Hempstead, NY 11549

5 Randall Division of Cell and Molecular Biophysics, King's College London, New Hunt's House, Guy's Campus, London SE1 1UL, UK

6 Department of Biosciences, University of Kent, Canterbury, Kent, CT2 7NJ, UK

* **Corresponding author. Email: jhale@nybc.org**

ABSTRACT

Spectrin tetramers of the membranes of enucleated mammalian erythrocytes play a critical role in red blood cell survival in circulation. One of the spectrins, αI , emerged in mammals with enucleated red cells following duplication of the ancestral α -spectrin gene common to all animals. The neofunctionalized αI -spectrin has moderate affinity for βI -spectrin, while αII -spectrin, expressed in non-erythroid cells, retains ancestral characteristics and has a 10-fold higher affinity for βI -spectrin. It has been hypothesized that this adaptation allows for rapid make-and-break of tetramers to accommodate membrane deformation. We have tested this hypothesis by generating mice with high-affinity spectrin tetramers formed by exchanging the site of tetramer formation in αI -spectrin (segments R0 and R1) for that of αII -spectrin. Erythrocytes with $\alpha II\beta I$ presented normal hematologic parameters yet showed increased thermostability and their membranes were significantly less deformable: under low shear forces they displayed tumbling behavior, rather than tank-treading. The membrane skeleton is more stable with $\alpha II\beta I$ and shows significantly less remodeling under deformation than red cell membranes of wild-type mice. These data demonstrate that spectrin tetramers undergo remodeling in intact erythrocytes and that this is required for the normal deformability of the erythrocyte membrane. We conclude that αI -spectrin represents evolutionary optimization of tetramer formation: neither higher affinity tetramers (as shown here) nor lower affinity (as seen in hemolytic disease), can support the membrane properties required for effective tissue oxygenation in circulation.

SIGNIFICANCE

Spectrin tetramers, made by the association of pairs of $\alpha\beta$ -spectrin dimers, are essential for red blood cell function. $\alpha I\beta I$ -spectrin tetramer is a unique feature of highly deformable enucleated mammalian red blood cells; $\alpha II\beta II$ is a more stable tetramer found in other tissues. Here, we have developed a mouse model to investigate the connection between low affinity red cell spectrin tetramer formation and cell deformability. Mice expressing the high affinity αII -spectrin binding site for βI -spectrin have erythrocytes with lower deformability than wild type. Lability of the $\alpha I\beta I$ spectrin tetramer at the self-association site enables membrane skeleton remodeling in intact red blood cells and is an essential component of the red cell deformability.

INTRODUCTION

Mammalian red blood cells are extremely deformable; this is a requirement for effective tissue oxygenation and to survive the large deformations experienced as they transverse the vasculature. Structurally, the red blood cell membrane is a composite material in which the spectrin-based membrane skeleton is anchored to the lipid bilayer via two major protein complexes: an ankyrin-based complex (containing, among other proteins, Band 3, Rh/RhAG and protein 4.2) and an actin-based complex (containing, among other proteins, 4.1R, adducin, dematin, Band 3, and glycophorin C) (1–3). The deformability of the red blood cell is a combination of mechanical properties of the cell membrane and excess surface area relative to its volume. While the structural organization of the various components of the red blood cell membrane is well described, the structural basis for its deformability is not fully understood (4).

Red cells undergo extensive elastic deformations during passage through the microvasculature while maintaining constant membrane surface area; the area dilation is energetically highly unfavorable. The principle resistance to area dilation (stretching) and bending is provided by the lipid bilayer, while the resistance to shear deformation is provided by the membrane skeleton that is anchored to the lipid bilayer (5).

Spectrin tetramers are the main structural component of the red blood cell membrane skeleton, consisting of two heterodimers of α I- and β I-spectrin interacting head-to-head at the dimer self-association site. Spectrins are polypeptides of multiple triple-helical repeats, 20 $\frac{1}{3}$ for α I-spectrin and 16 $\frac{2}{3}$ for the shorter β I-spectrin (6, 7). At the self-association site, the single helix of the R0 repeat at the N-terminus of α I-spectrin interacts with the two helices of the R17 repeat at the C-terminus of β I-spectrin forming a complete triple helical repeat (8–10).

α I and β I erythrocyte spectrins are members of a family of proteins encoded by multiple genes in mammals: two encode α -spectrin and five encode β -spectrin. All spectrins can form tetramers ($\alpha_2\beta_2$) by self-association of spectrin $\alpha\beta$ dimers (11). The relative strength of spectrin dimer interaction at the self-association site differs markedly between the erythroid α I- β I spectrin and the abundant α II- β II spectrin found in solid tissues, with α II- β II spectrin tetramers being significantly more stable (11). The significance of the reduced strength of erythroid dimer self-association remains unclear: one current hypothesis is that it allows rearrangement of the membrane skeleton under the shear force experienced in the circulation (4).

Through phylogenetic analysis, Salomao et al (12) showed that the gene encoding α I-spectrin is the result of duplication of the ancestral α -spectrin common to all animals. The duplication event was coincident with the emergence of mammals. One of the resulting pair, α II-spectrin, retained the ancestral characteristics of high thermal and mechanical stability (11), together with high affinity binding to spectrin β -chains (11). The other of the pair, α I-spectrin, was neofunctionalized for highly deformable, enucleated erythrocytes: it has a more flexible structure deriving from lower stability of some of its triple helical repeats (12), and lower affinity binding to β -chains (11). The precise nature of the physiological benefits of this neofunctionalization, the lower affinity for β -chains, and how they relate to the advantages of enucleated erythrocytes, are not clear.

In the present study, we explored the contribution of the binding strength of $\alpha\beta$ dimer at the self-association site to the biophysical properties of the red blood cell membrane. To achieve this, we generated a genetically modified mouse model in which the α I-spectrin self-association domain was exchanged for the α II-spectrin self-association domain. These mice are viable and do not present with significant anemia. Functional characterization of the genetically modified red cells showed that increasing the strength of the spectrin dimer self-association results in significantly reduced membrane deformability, with marked reduction in deformation-induced remodeling of the spectrin skeleton of intact red cells. We conclude that α I-spectrin represents evolutionary optimization of spectrin dynamics to support the unique membrane requirements of mammalian erythrocytes in circulation.

MATERIALS AND METHODS

Generation of alpha II spectrin knock-in mice.

α II-spectrin knock-in mice were generated by the inGenious Targeting Laboratory, Inc (NJ). Exons 1, 2, 3 and part of exon 4 of the *Spta1* gene spanning ~ 5.9 kb region were replaced with the exons 2, 3 and part of exon 4 of the *Sptan1* spanning ~ 4.9 kb region. The mice were initially generated as 129 x C57 hybrid and backcrossed for at least 10 generations into a C57BL/6 background. In experiments involving wild type mice, pure C57BL/6 inbred mice were used. All animals were at least 3 months of age. Both sexes were used, and we did not observe differences between males and females. The mice were maintained at the animal facility of New York Blood Center under specific-pathogen-free conditions according to institutional guidelines. Animal protocols were reviewed and approved by the Institutional Animal Care and Use Committee.

Genotyping.

Genomic DNA was extracted from mouse-tails. *Genotyping* was performed by multiplex PCR. The α I spectrin allele was amplified using primers: α I FOR: 5'-ATG GAA ACT CCA AAG GAA ACT GTG

AGT A-3' and α I REV: 5'-GTC ATT CCA CAA GAG CAC AAT TTT TAG T -3'. Similarly, the α II spectrin allele was amplified using primers: α II FOR: 5-CAT TAT ACG AAG TTA TGG TAC CTG CAG-3' and α II REV: 5'-TCA ATT CCT AGT ACT CTG TCT GCC TCC-3'.

Generation of anti-spectrin antibodies.

Polyclonal antibody against α I-spectrin N-terminus, α I-spectrin C-terminus, or α II spectrin N-terminus was raised in rabbit using recombinant α I N-terminus, α I 20-C or α II N-terminus as antigen. The antibodies were affinity purified on Sulfolink Coupling Resin (Pierce Biotechnology, Inc.). Antibody specificity was examined by Western blotting using the corresponding recombinant protein.

Characterization α -spectrin in α II β I mice red cells.

The red cells of the α II β I mice were characterized by native gels and western blot analysis. Ghosts prepared by lysis of red cells in ice-cold hypotonic buffer A (5 mM Tris/5 mM potassium chloride, pH 7.4) were twice washed in the same buffer, and twice more with extraction medium (Buffer B: 0.25 mM sodium phosphate, pH 7.4). Spectrin was extracted by overnight dialysis at 4 °C in buffer B and recovered in the supernatant after centrifugation for 20 min at 20,000 g. Protein concentration was determined spectrophotometrically, taking $E(280 \text{ nm}; 1 \text{ mg ml}^{-1}; 1 \text{ cm}) = 1.07$. The extracted spectrin was then examined by gel electrophoresis in the native state in a Tris-Bicine buffer system, run in the cold (13) and stained with GelCode Blue. Membrane proteins from whole RBC ghosts separated by sodium dodecyl sulfate-polyacrylamide gel electrophoresis (SDS-PAGE) in 4% polyacrylamide gels and were transferred to nitrocellulose membrane (Bio-Rad). Membranes were blocked for 1 hour in PBS-T (PBS+0.1% Tween 20), containing 4% nonfat milk and 1% BSA. Followed by 1-hour incubation with relevant α -spectrin primary antibodies. Following washing with PBS-T, the nitrocellulose membrane was incubated with the horseradish peroxidase [HRP] conjugated secondary antibody (anti-rabbit). Immunoblots were visualized using the G:BOX gel imager (Imgen Technologies, NY) by the enhanced chemiluminescence method.

Preparation of Recombinant α II-spectrin fragment.

The cDNA encoding the N-terminal region of nonerythroid α II-spectrin (amino acids 1-149) was expressed from the vector pGEX-2T, as described previously (11). The fragment was purified on glutathione-Sepharose column, dialyzed, and concentrated using Centricon Plus-70 centrifugal filter units (Sigma Aldrich).

Incorporation of α II-spectrin fragment into Erythrocyte Ghosts.

Total blood was obtained from wild type or α II-spectrin knock in mice by cardiac puncture. Red cells were washed three times in ice-cold isotonic buffer and then lysed in 35 volumes of ice-cold buffer A to obtain ghosts. After three washes in 35 volumes of buffer A, ghosts (5×10^9 /mL) were incubated with the indicated concentrations of α II-spectrin fragment for 10 minutes on ice. Isotonicity was restored by adding 0.1 volume of 1.5M potassium chloride, pH7.4 for 10 minutes on ice and ghosts were resealed by incubating them at 37°C for 40 minutes.

Extraction and Analysis of Spectrin from Resealed Ghosts.

After resealing, the ghosts were lysed again in 35 volumes of Buffer A. 10 μ l of packed ghosts were washed three times in isotonic saline and were subjected to SDS-PAGE and western blot with an anti-GST antibody to confirm incorporation of the α II-spectrin fragment. The remaining ghost population was washed two additional times in ice-cold Buffer A and spectrin was then extracted in Buffer B overnight at 4°C. After centrifugation (20,000g, 20 minutes), the spectrin tetramer, dimer and their complexes with the α II-spectrin fragment were resolved by gel electrophoresis in a Tris-Bicine buffer system run in the cold (13).

Measurements of red cell deformability by ektacytometry.

Blood (50-200 μ l) was drawn from mice via tail, submandibular vein (survival) or cardiac puncture (non-survival). Red blood cell deformability was measured using an ektacytometer as previously described (14). Red blood cells (RBC) were suspended in 4% Polyvinylpyrrolidone (PVP, 360 kDa) PBS solution (5 ml PBS-PVP + 25 μ l whole blood) and deformed in a Couette viscometer, in which the outside cylinder is spun to obtain defined values of applied shear stress. The change in the laser diffraction pattern of the erythrocytes was recorded while they were subjected to increasing values of applied shear stress (0-30 Pa). The ratio of principal axes of the elliptically shaped diffraction pattern designated deformability index (DI) is a measure of the extent of cell deformation. The biomechanical origin of the shape of the DI curve is complex but the reproducibility and certain characteristics are useful measures of the deformability of the red cell. At DI_{max} the value of the DI attained at the maximum value of applied shear stress of 30 Pa, is a measure of cellular deformability. Decreased values of DI_{max} reflect decreased surface area and hence increased sphericity of RBCs. As the rate of change of the DI at lower shear rates is a good indicator of the red cell membrane stiffness, illustrated best in the Eadie-Hofstee transformation of the DI curve (15). Linear fitting of the Eadie-Hofstee transformed data allowed the maximum deformation index (DI_{max}) and shear stress at half max deformation ($SS_{1/2}$) to be extracted (15, 16).

Rheoscope imaging.

Deformation of red cells from WT and $\alpha\text{II}\beta\text{I}$ mice in Couette flow were observed and imaged in a transparent counter-rotating cone and plate rheoscope (17) (model MR-1, Myrenne Instruments, CA) with a cone angle of 2° , mounted on a Leitz Diavert inverted microscope using a Leitz long distance 32x (NA 0.4) objective. 5 μl whole blood in 1ml 8% PVP-PBS solution and a series of observations were made across the full speed range 1 to 43 RPM of the instrument. The images were taken using a Nikon DS-Qi camera with a 1 ms exposure.

Osmotic fragility analysis.

5 μl of packed RBCs were suspended in 2 ml of NaCl solutions of varying osmolarities and incubated for 20 minutes at room temperature. Following low-speed centrifugation (200 g, 3min), the absorbance of the supernatant was measured at 540 nm to quantify the released hemoglobin. The absorbance at 540 nm for the different osmolarities was normalized against complete red blood cell lysis using water (18).

Thermal Sensitivity.

Whole blood was washed 3 times in PBS, 5 μl of packed RBCs were suspended in 1 ml of PBS and 100 μl aliquoted into 10 PCR tubes. The tubes were heated using a gradient capable PCR thermal cycler and the block was heated to 45°C for 1 min and $45\text{-}50^\circ\text{C}$ gradient for another 15 mins. Heated cells were fixed adding 100 μl of 2% glutaraldehyde in PBS to each tube. The samples were examined for echinocytic and spherocytic cells by phase contrast microscopy and the numbers of normal and abnormal cells counted (19).

Blood analyses.

Whole blood collected from wild type (WT) or $\alpha\text{II}\beta\text{I}$ mice using EDTA (ethylenediaminetetraacetic acid)-coated capillary from the retro-orbital sinus. Complete blood counts were obtained using the ADVIA 120 Hematology System (Siemens, Germany).

Optical Microscopy.

High resolution images of intact red blood cells from WT and $\alpha\text{II}\beta\text{I}$ mice were acquired using a Nikon DS-Qi camera mounted on a Nikon Ti-U inverted microscope with a Soret band filter (413nm, 10nm) (Edmund Optics, NJ) (20).

Fluorescence imaged micropipette deformation (FIMD).

The density distribution of proteins within the red cell membrane during deformation was measured using the combination of fluorescent imaging and micropipette aspiration as described by Discher et al (21),

with some additional modifications. Whole blood was washed three times in mouse-PBS (MPBS) (10 mM NaCl, 155 mM KCl, 10 mM glucose, 1 mM MgCl₂, 2.5 mM KHPO₄, pH 7.4) (22). Band 3 was chemically labeled using methods previously described (23). Briefly, 5 μ l of packed RBCs were incubated in 200 μ l of 80 μ g/ μ l Alexa Fluor 488 C₅ Maleimide (Life Technologies, NY) in MPBS for 40 minutes. They were washed three times in MPBS and then suspended at 1 μ l packed cells per ml MPBS + 0.1% bovine serum albumin. The labeled RBC suspension was injected into an imaging chamber consisting of a microscope slide and coverslip separated by four layers of parafilm. Individual cells were aspirated into glass micropipettes with internal diameters between 1-2 μ m. The micropipettes were pulled from glass capillary tubing using a Sutter P-1000 micropipette puller (Sutter, Novato, CA, USA) and cut to the required diameters using a home built micro-forge. The micropipettes were back filled using a Microfil capillary (World Precision Instruments, Sarasota, FL, USA) with MPBS and connected to a manometer to control the aspiration pressure. The applied pressure was sufficient to aspirate the cell to the extent that the aspirated portion of the cell was maximal for the available surface area, and the proportion of the cell membrane outside the pipette was a sphere.

In the present study, the aspiration length was adjusted by exchanging the suspending solution while individual cells were held in the micropipette. By using computer-controlled syringe pumps exchanging the PBS buffer between solutions of 250 mOsmol and 150 mOsmol enabled imaging of a single cell through a range of aspirated tongue lengths. Fluorescent images of the aspirated RBCs were acquired using a Nikon DS-Qi camera mounted on a Nikon Ti-U inverted microscope. All image analysis was done in ImageJ (24) and semi-automated with custom plugins. From measurements of the normalized aspiration length (L/R_p), the outside sphere radius (R_s), the normalized intensity profile along the aspiration, as well as the entrance intensity (ρ_e), and cap intensity (ρ_c) were computed.

Statistics

The presented data is obtained from at least three independent experiments using blood from at least three individual mice. Statistical significance was determined by two-tail t-tests for unpaired samples with $\alpha=0.05$. Data is expressed as the mean \pm SD (standard deviation), P-values > 0.05 were considered statistically significant, and indicated by asterisks (* $P \leq 0.05$, ** $P \leq 0.01$, *** $P \leq 0.001$).

RESULTS

Generation and characterization of α II β I knock-in mice.

To assess contribution of the binding strength of $\alpha\beta$ dimer at the self-association site on the mechanical properties of the red blood cell membrane, a knock-in strain of mice was generated in which the labile α I- β I spectrin tetramer was replaced by much higher affinity α II- β I spectrin tetramer by exchanging exons 2-

4 of α I-spectrin (*Spta1*) with the corresponding exons of α II-spectrin (*Sptan1*). This results in mouse red cells, which express hybrid α -spectrin protein in the erythrocyte that has the N-terminus domains R0 and R1 from α II-spectrin in place of the N-terminus domains R0 and R1 from α I-spectrin. R0 and R1 N-terminus domain interacts with the C-terminal domain of β -spectrin to form the heterodimer and one half or the spectrin tetramer as illustrated in Fig. 1A.

The genotypes of all mice were determined by PCR. Amplification with the primer pairs used produced a 340 bp fragment in WT mice and 700 bp fragment in the α II β I knock-in mouse. While 340 bp fragment was a feature of WT mice the homozygous knock-in mice showed only the 700 bp fragment while, as expected, heterozygous knock-in mice showed both fragments (Fig. S1).

Further validation of the knock-in of the hybrid α -spectrin was shown by SDS gel and western blot analysis of red blood cell membrane ghosts from WT and homozygous α II β I mice (Fig. S2). The overall patterns of proteins revealed in Coomassie blue-stained SDS gels (Fig. 1B, *left panel*) appeared essentially identical between the strains, indicating that the knock-in does not result in any major change to overall protein composition of the membranes. Antibody to N-terminus of α I-spectrin but not the antibody to N-terminus of α II-spectrin recognized spectrin of red cells of WT mice (Fig. S2). In contrast, and as expected, only the antibody to N-terminus of α II-spectrin but not antibody to N-terminus of α I-spectrin recognized spectrin of red cells of homozygous α II β I mice. Importantly, antibody to C-terminus of α I-spectrin recognized spectrin in red cells of both WT and α II β I mice. Thus, the knock-in strategy used successfully generated a full-length hybrid α I-spectrin with self-association domain of N-terminus of α II-spectrin in the red cells of α II β I mice.

Complete blood counts by Advia 120 hematology analyzer demonstrated normal indices with no significant differences between WT and α II β I mice (Table S1). Although statistically significant differences in red cell count, hemoglobin concentration and hematocrit are observed between the WT and α II β I mice the difference is small and well within normal parameters for normal healthy mice and would be only considered to be very mildly anemic (25). In addition, both WT and α II β I mice presented similar erythrocyte morphology both appearing as normal biconcave discocytes as shown in the representative microscopy images in Fig. 1B.

Previous studies have reported altered erythrocyte membrane deformability despite normal red cell parameters (26). The formation of spectrin dimers, tetramers and higher order oligomers in intact membranes was assessed by extracting the spectrin from isolated membranes under conditions that preserve its native state, i.e. using very low ionic strength media at 4°C. The resulting extracts were

analyzed by non-denaturing gel electrophoresis (Fig. 1C). As expected, the spectrin extracts from wild type mice showed mainly tetramers with some dimers but without indication of higher order oligomers. Extracts from α II β I mice showed similar tetramer composition but with no measurable dimers, instead showing a band indicating enhanced higher oligomer formation. Note also that the tetramer in the α II β I mice extracts has a faster electrophoretic mobility than wild type, consistent with the genetic modification leading to a small change in the overall conformation of the tetramer.

Univalent fragments of α -spectrin, containing the dimer self-association site, are known to bind to spectrin on the membrane as tetramers undergo dynamic association and dissociation (5, 12). If spectrin tetramers in intact membranes are more dynamic in wild type than α II β I, then an exogenous α II-spectrin peptide fragment should incorporate more readily into wild type than α II β I membranes. To test this, the α II-peptide was added to ghosts from wild type or α II β I cells; the ghosts were resealed and incubated at 37°C to promote incorporation of the peptide. Fig. 1D shows significant incorporation of the fragment into the spectrin of wild type ghosts; by contrast spectrin from α II β I incorporated little-to-none. This result is consistent with α II β I tetramers being much less labile than wild type.

Surface area of α II β I and WT RBCs.

The surface area of red cells was measured geometrically using micropipette aspiration method (27, 28). For α II β I cells it was $102.2 \pm 7.6 \mu\text{m}^2$, an approximately 10% loss compared to that of WT mice, $111.5 \pm 6.2 \mu\text{m}^2$ (Fig. 2A). Osmotic fragility of RBCs was measured by exposure to hypotonic stress by suspending in low ionic strength buffer solutions (Fig. 2B). RBCs from α II β I mice show significantly less resistance to hemolysis with 50% lysis at 150 mOsm/kg in contrast to 50% lysis at 130 mOsm/kg of RBCs from WT mice. Resistance to hemolysis is primarily defined by cell surface area to volume ratio (cell sphericity) (29, 30) and we conclude that increased osmotic fragility arises from increased sphericity α II β I cells consistent with their decreased cell surface area.

Thermal sensitivity of α II β I knock-in and WT RBCs.

Erythrocytes have been shown to have particular sensitivity to temperature (19, 31). While human RBCs maintain their discoid morphology upon heating to 48 °C, increasing the temperature to 49 to 50 °C induces rapid shape transition with membrane fragmentation and generation of spherocytes (19). Diluted suspensions of RBCs from α II β I and WT mice were heated to temperatures between 45-50 °C. The RBCs from WT mice began to transform to echinocytes (crenated) at 47 °C with significant crenations between 48-49 °C and were 100% spherocytic at 49 °C (Fig. 3A), with 50% of RBCs crenating at 48.4 °C. In contrast, RBCs of α II β I mice did not start to crenate until 48-49 °C with significant crenation not occurring to >48.5 °C, with 50% crenated RBCs occurring at 49.5 °C. At 50 °C α II β I RBCs did not reach

100% spherocyte cells. Shown in Fig. 3B are brightfield images of heat-induced morphological changes in RBCs of both WT and $\alpha\text{II}\beta\text{I}$ samples between 47 and 49 °C. These findings imply that the more stable dimer-dimer interaction of $\alpha\text{II}\beta\text{I}$ bestows increased thermal resistance to RBCs of $\alpha\text{II}\beta\text{I}$ knock-in mice.

Deformability of RBCs as assessed by Couette flow.

The effect of the modified $\alpha\text{II}\beta\text{I}$ dimer on the deformability of red cells was measured by ektacytometry (14). The maximal deformability index at the highest shear stress (DI_{max}) in the higher suspending medium viscosity reached a plateau defined as DI_{max} which is less for the $\alpha\text{II}\beta\text{I}$ mice samples (DI_{max} 0.67 ± 0.015) compared to the WT samples (DI_{max} 0.75 ± 0.015) as shown in Fig. 4A (student t-test, $p=4.2\times 10^{-5}$). As the maximum DI should be only limited by the membrane surface area of the RBCs provided the shearing does not result in cell fragmentation and loss of membrane area, the noted decrease in DI_{max} is the result of $\sim 10\%$ decrease in surface area of $\alpha\text{II}\beta\text{I}$ mice red cells. Importantly, the peak DI of the $\alpha\text{II}\beta\text{I}$ cells did not reach a plateau at the maximum applied shear stress of the instrument in the suspending medium of lower viscosity, (indicated in the Eadie-Hofstee transformed data shown in Fig. 4B). The $\alpha\text{II}\beta\text{I}$ cells clearly need significantly greater shear force to deform to the same extent as the WT cells. For example, the WT cells reach half their maximum deformation ($\text{SS}_{1/2}$) at a shear stress of 1.13 ± 0.097 Pa while the $\alpha\text{II}\beta\text{I}$ samples needed a shear stress of 8.54 ± 0.51 Pa (student t-test, $p=2.9\times 10^{-6}$) to reach the same extent of deformation, implying decreased membrane deformability (32). Additionally, at low shear stresses < 1 Pa the $\alpha\text{II}\beta\text{I}$ cells did not undergo tank-threading but instead showed DI values consistent with cell tumbling (33, 34).

This behavior is further demonstrated in the images of the red cells of deformed by the rheoscope in Fig. 4C. In those, $\alpha\text{II}\beta\text{I}$ red blood cells have significant resistance to shear deformation compared to WT mice. WT red blood cells tank-tread even at very low shear stress 0.4 Pa while the $\alpha\text{II}\beta\text{I}$ red cells require shear stress > 2 Pa to start tank-treading.

Membrane skeleton density of deformed $\alpha\text{II}\beta\text{I}$ and WT as assessed by fluorescence-imaged microdeformation.

Fluorescence-imaged microdeformation developed by Discher et al (21, 23) is an effective way to determine the connectivity of membrane proteins such as band 3 to the underlying membrane skeleton. The method typically involves imaging many cells suspended in isotonic buffer aspirated into micropipette with increasing aspiration pressures to determining the entrance (ρ_e) and cap (ρ_c) densities as a function of the aspirated cell length (Fig. 5A). Changing the osmolality of the buffer in the chamber while the cell is aspirated in the micropipette enables the measurement of ρ_e and ρ_c at many aspiration lengths for each cell (Movie S1). The ratio of ρ_e and ρ_c for band 3 in the $\alpha\text{II}\beta\text{I}$ cells using this strategy

showed a significantly steeper gradient than that seen for WT cells (Fig. 5B). As the measured band 3 density correlates to the membrane skeletal density distribution, this finding implies that increased affinity of spectrin interaction at the self-association site results in greater resistance to membrane skeleton remodeling. Fitting equation (1) below for the band 3 density data obtained for each aspirated cell where K is the area dilation modulus, μ shear modulus, R_p micropipette radius and L the aspiration length; a value for the parameter (K/μ) can be derived. For the α II β I cells the ratio of the area stretch and shear moduli (K/μ) was determined to be 1.10 ± 0.22 ($n=14$) compared to 1.99 ± 0.32 ($n=8$) for WT cells (student t-test, $p=4.4 \times 10^{-5}$) (21, 23).

$$\frac{L}{R_p} = \frac{K}{\mu} \left\{ \left(\frac{3}{4} \right) \left[1 - \left(\frac{\rho_c}{\rho_e} \right)^2 \right] + \left(\frac{\rho_e}{2\rho_c} \right) \ln \left(\frac{\rho_e}{\rho_c} \right) \right\} + \ln \left(\frac{\rho_e}{\rho_c} \right) \quad (1)$$

In the absence or reduction of remodeling, the membrane skeleton undergoes a larger shear deformation before breakage of the spectrin self-association site, and this will be reflected by higher ρ_e intensity. Indeed, the intensity at the micropipette entrance ρ_e is increased for all aspirated α II β I red cells compared to the WT cells while the ρ_c intensity showed much smaller difference between the two cell types (Fig. 6A). This is a result of the difference in the dominant type of deformation of the membrane skeleton at the pipette entrance and cap of the aspirated cell. At the micropipette entrance, skeletal deformation is mainly due to shear deformation, while at the cap the deformation is dominated by area-dilation. ρ_c shows only a small difference intensity between the WT $\rho_c=0.622 \pm 0.050$ compared to 0.525 ± 0.072 for the α II β I cells at $L/R_p=6$ (student t-test, $p=0.0016$). This indicates the maximum area dilation of membrane skeleton is approximately the same, suggesting the maximum area extension of the membrane skeleton is constant, consistent with a spectrin tetramer length invariance between the two cell types. By contrast, ρ_e was significantly different between WT and α II β I cells: at $L/R_p=6$, WT ρ_e intensity was 1.71 ± 0.054 , compared to 2.15 ± 0.098 for the α II β I cells (student t-test, $p=0.0025$). This is consistent with a changed rate of remodeling spectrin tetramers in α II β I cells.

Estimates of the principle stretch ratios of the membrane skeleton can be determined from the relative membrane skeleton density using methods described previously (21, 23, 35). Briefly, by conservation of mass and considering the aspirated tongue to be an axisymmetric deformation of a portion of a spherical surface radius R_0 with uniform density, Equation 2 can be used to estimate the principle stretch ratio λ_2 and then λ_1 .

$$\lambda_1 = 1/(\bar{\rho}\lambda_2)$$

$$\lambda_2(z') = \frac{r(z')}{R_p} \left\{ \left(\frac{R_0}{R_p} \right)^2 - \left[\left(\frac{R_0}{R_p} \right) - \left(\frac{1}{R_0} \right) \int_{pole}^{z'} \rho_{net} dz' \right]^2 \right\}^{-1/2} \quad (2)$$

Since the intensity gradients of the aspirated portions of the cells are nearly perfectly linear, the mean ρ_e and ρ_c for a give aspiration length ($L=6$) for each sample are used to model ρ intensity profile to calculate the principle stretches shown in Fig. 6B. Using this method, we find in WT cells $\lambda_1=2.18\pm 0.069$, $\lambda_2=0.268\pm 0.006$ at pipette entrance and $\lambda_1=\lambda_2=1.27\pm 0.054$ at cap while in $\alpha\text{II}\beta\text{I}$ cells $\lambda_1=1.86\pm 0.080$ (student t-test, $p=1.5\times 10^{-10}$), $\lambda_2=0.251\pm 0.008$ (student t-test, $p=4.8\times 10^{-7}$) at pipette entrance $\lambda_1=\lambda_2=1.38\pm 0.11$ (student t-test, $p=0.003$) at cap. Findings from all these analyses are consistent with the hypothesis that spectrin tetramers undergo less remodeling in $\alpha\text{II}\beta\text{I}$ membranes than WT, and that remodeling requires making and breaking tetramers. WT membranes are more susceptible to deformation than $\alpha\text{II}\beta\text{I}$ membranes because remodeling can accommodate larger strain.

DISCUSSION

αI -spectrin emerged with the appearance of mammals, and apparently coincident with the processes that allow enucleation of erythrocyte precursors and the circulation of mature enucleated erythrocytes. In earlier work, with fewer genomes than are now available, we noted the absence of αI -spectrin from all other vertebrates sequenced at that time (12). Subsequent sequencing of genomes of many more animals confirms this thesis. In particular, mammals are amniotes: the other amniotes are the birds and reptiles. Large numbers of bird and reptile genomes are now available: none of them encode αI -spectrin, although all encode the ancestral α -spectrin, which is retained in mammals as αII -spectrin.

These observations pose several questions about the physiological advantages obtained through the neofunctionalization of αI -spectrin. For example, is it part of, or required for, the process of enucleation? Alternatively (or in addition), is the low affinity interaction with β -spectrin essential for the physiology of mature enucleated erythrocytes? In the present study, we address this by exchanging the low affinity-binding site for β -spectrin in αI -spectrin for the high affinity-binding site in αII -spectrin. The resulting $\alpha\text{I}/\alpha\text{II}$ chimeras clearly retain the ability, first, to form dimers with β -spectrin by side-to-side association, and, secondly, to form tetramers by head-to-head association of dimers. Mature enucleated red cells form in the chimeric mice, indicating no indispensable role for αI -spectrin in the process of enucleation.

In broad terms, the overall properties of the chimeric spectrin are not grossly altered. The modification of spectrin does not result in phenotypes associated with anemia in humans. The $\alpha\text{II}\beta\text{I}$ mice are not deficient in spectrin, and membrane loss is small ($<10\%$) which results in increased osmotic fragility, probably a

result of reduced remodeling in the $\alpha\text{II}\beta\text{I}$ mice. The change in osmotic fragility is also minor compared to the more substantial increase in fragility seen in hereditary spherocytosis (HS) patients (36). Also, the osmotic fragility curve for the $\alpha\text{II}\beta\text{I}$ mice does not have the shoulder seen for HS samples as the heterogeneity of sphericity of the HS red cells is much broader than that noted in $\alpha\text{II}\beta\text{I}$ mice. Severe forms of hereditary elliptocytosis arise from mutations in αI - and βI -spectrin which inhibit tetramer formation (37, 38): elliptocytes were absent in the $\alpha\text{II}\beta\text{I}$ mice. A clinically severe form of elliptocytosis, hereditary pyropoikilocytosis (HPP), arising from mutations at the self-association site that markedly weakens spectrin dimer self-association enhance heat sensitivity of red cells (39, 40). The weakened self-association site in HPP causes RBCs to fragment at 45 °C compared to 50 °C for normal human red cells (40). In marked contrast, red cells of the $\alpha\text{II}\beta\text{I}$ mice show increased thermal stability: shape changes occurring at 49.5 °C, 0.9 °C higher than that noted for wild-type normal red cells. Additionally, electrophoresis by non-denaturing gels of HPP patient samples shows a shift from spectrin tetramers to dimers (39), while $\alpha\text{II}\beta\text{I}$ red cells show the opposite, with a shift to higher oligomers.

As measured by ektacytometry, there is a marked change in membrane deformability of $\alpha\text{II}\beta\text{I}$ red cells; however, the difference in DI_{max} is small, consistent with the relatively minor loss of membrane area. Membrane deformability as reflected by the $\text{SS}_{1/2}$ parameter is 7.6 \times greater for the $\alpha\text{II}\beta\text{I}$ red cells compared to normal red cells, clearly demonstrating the importance of the strength of dimer self-association to red cell membrane deformability. Distinctly different from the ektacytometry of HS red cells (in which DI_{max} is markedly decreased) that decrease in DI_{max} is much less for red cells for $\alpha\text{II}\beta\text{I}$ mice. However, while the rate of change in DI or $\text{SS}_{1/2}$ for HS and normal human red cells are very similar, the rate of change in DI is significantly less for $\alpha\text{II}\beta\text{I}$ red cells compared to normal red cells at low shear rates 0-10 Pa (41–43). At low shear stresses, <1 Pa, the deformability profiles of $\alpha\text{II}\beta\text{I}$ red cells are consistent with red cell tumbling and swinging, and not tank-treading (33, 34, 44). This is consistent with the images of the deformed red cells in the rheoscope showing the resistance $\alpha\text{II}\beta\text{I}$ red cells to deformation. This has been previously observed in more rigid cells (33, 34) and theoretical models of such behavior (45, 46).

The K/μ ratio measured by fluorescence imaged micro-deformation, of $\alpha\text{II}\beta\text{I}$ mice red cells was ~80% less than those from normal wild-type mice. In computer simulations of erythrocyte membranes, Boal showed $\text{K}/\mu=2$ for six-fold networks of simple harmonic springs (47); similarly, modelling by Hansen et al (48) revealed that decreasing the connectivity of the network increased K/μ . The simplest interpretation of our K/μ measurements is that $\alpha\text{II}\beta\text{I}$ mice have increased connectivity in the cytoskeletal network, arising from enhanced interaction of spectrin dimers at the self-association site.

Electron microscopy studies of α II-spectrin and α I-spectrin have shown α II-spectrin to be a stiffer rod-like molecule compared to α I-spectrin (49, 50). Since the spectrin modification in α II β I mice is small ($1\frac{1}{3}$ repeats of the $20\frac{1}{3}$ repeats) the modified polypeptide structure is largely unchanged and the flexibility of α I-spectrin is retained. If modeled as a simple harmonic spring network, the spring constant would be essentially same in both the α II β I and the wild type. Therefore, the differences in membrane skeleton μ , shear and K, area dilation moduli observed between the α II β I, and the wild-type are best explained by membrane skeleton remodeling (i.e. by making and breaking tetramers) resulting in reduced connectivity in the wild-type compared to the α II β I model.

The higher oligomers observed in the α II β I mice could also contribute to the change in the mechanical properties of the membrane skeleton. The significant difference in the incorporation of α II-spectrin into the membrane clearly indicate that the change in binding strength at the self-association site is the dominant factor in the observed change in mechanical properties of the membrane skeleton in the α II β I mice.

Almost all the computational and theoretical models of membrane biophysical properties ignore spectrin remodeling coming from breaking and reforming tetramers and it is often absorbed in the shear modulus terms; this is largely due to the complexity of including this feature in the models. Recent attempts to model red blood cell membranes (51, 52) have begun to include this contribution and, while giving improved understanding of red cell properties, data presented here can be incorporated into theoretical models to refine them further. This will inform future understanding of cell fragmentation and life span in clinical settings, as well as understanding of evolutionary processes underlying the biology of blood circulation.

In relation to the evolution of spectrin gene function, it appears the ancestral α -spectrin underwent duplication at about the time mammals emerged, followed by selective adaptation of each, especially α I-spectrin. Gene pairs may become subfunctionalized, for example, by alterations to expression. In the case of mammalian α spectrins, α II-spectrin is expressed in the vast majority of cell types other than erythrocytes; in erythrocytes, α I alone carries out α -spectrin function.

Subfunctionalization is often the precursor to neofunctionalization (53), since functions can subsequently be adapted separately. In the case of α I-spectrin, we argued in earlier work (12) that the rapid make-and-break of spectrin tetramers in erythrocyte membranes represents a new function. Data presented here extend and bring new insight to this concept and demonstrate that the ancestral high affinity spectrin tetramers cannot provide the erythrocyte plasma membrane with the deformability under shear stress

required physiologically. We view promotion of erythrocyte deformability as a new function of α I-spectrin that was not provided by the ancestral (α II) spectrin, hence α I-spectrin is neofunctionalized.

While neofunctionalization was the end point, the simplest path to getting there may have been neutral drift of one of the pair of duplicates after separation of expression (i.e. asymmetric evolution (54)), to the point where any further reduction of affinity for β I-spectrin impaired red cell survival. The point at which neutral drift resulted in weaker—but optimal—affinity of α I-spectrin for β I-spectrin represented the point of neofunctionalization. Once this point had been reached in an early mammal, it appears to have been strongly favored in subsequent evolution: every amino acid in α I-spectrin at the interface with β I-spectrin (PDB:3LBX) has been conserved since the last common ancestor of humans and platypus, around 180 million years ago.

CONCLUSIONS

In conclusion, our findings reveal that spectrin tetramers are dynamic at the self-association site in intact red blood cells, and that remodeling of the membrane skeleton is an essential component of the normal mechanical properties of red blood cells. Mammalian erythrocytes have a form of spectrin optimized for rapid make-and-break of tetramers and cannot tolerate either higher or lower affinity spectrin tetramers for normal biophysical function.

AUTHOR CONTRIBUTIONS

J.H., X.A., W.G., A.B. and N.M. – designed research, J.H., X.G., E.G., J.P., and L.B. – performed research, J.H., L.B., W.G., A.B., C.H. and N.M. – analyzed data, J.H., C.H., W.G., A.B. and N.M. – wrote the paper.

ACKNOWLEDGMENTS

This work was supported in part by National Institute of Diabetes and Digestive and Kidney Diseases grant DK32094.

REFERENCES

1. Mohandas, N., and P.G. Gallagher. 2008. Red cell membrane: past, present, and future. *Blood*. 112:3939–48.
2. Burton, N.M., and L.J. Bruce. 2011. Modelling the structure of the red cell membrane. *Cell*. 215:200–215.
3. Bennett, V., and A.J. Baines. 2001. Spectrin and ankyrin-based pathways: metazoan inventions for integrating cells into tissues. *Physiol. Rev.* 81:1353–92.
4. Lux, S.E. 2016. Anatomy of the red cell membrane skeleton: unanswered questions. *Blood*. 127:187–199.
5. An, X., M.C. Lecomte, J.A. Chasis, N. Mohandas, and W. Gratzer. 2002. Shear-response of the spectrin dimer-tetramer equilibrium in the red blood cell membrane. *J. Biol. Chem.* 277:31796–800.
6. Speicher, D.W., G. Davis, and V.T. Marchesi. 1983. Structure of human erythrocyte spectrin. II. The sequence of the alpha-I domain. *J. Biol. Chem.* 258:14938–47.
7. Yan, Y., E. Winograd, A. Viel, T. Cronin, S.C. Harrison, and D. Branton. 1993. Crystal structure of the repetitive segments of spectrin. *Science (80-)*. 262:2027–2030.
8. Ursitti, J.A., L. Kotula, T.M. DeSilva, P.J. Curtis, and D.W. Speicher. 1996. Mapping the human erythrocyte β -spectrin dimer initiation site using recombinant peptides and correlation of its phasing with the α -actinin dimer site. *J. Biol. Chem.* 271:6636–6644.
9. Viel, A., M.S. Gee, L. Tomooka, and D. Branton. 1998. Motifs involved in interchain binding at the tail-end of spectrin. *Biochim. Biophys. Acta - Protein Struct. Mol. Enzymol.* 1384:396–404.
10. Hill, S.A., L.G. Kwa, S.L. Shammas, J.C. Lee, and J. Clarke. 2014. Mechanism of assembly of the non-covalent spectrin tetramerization domain from intrinsically disordered partners. *J. Mol. Biol.* 426:21–35.
11. Bignone, P.A., and A.J. Baines. 2003. Spectrin alpha II and beta II isoforms interact with high affinity at the tetramerization site. *Biochem. J.* 374:613–24.
12. Salomao, M., X. An, X. Guo, W.B. Gratzer, N. Mohandas, and A.J. Baines. 2006. Mammalian alpha I-spectrin is a neofunctionalized polypeptide adapted to small highly deformable erythrocytes. *Proc. Natl. Acad. Sci. U. S. A.* 103:643–648.
13. Shahbakhti, F., and W.B. Gratzer. 1986. Analysis of the Self-Association of Human Red Cell Spectrin. *Biochemistry.* 25:5969–5975.
14. Groner, W., N. Mohandas, and M. Bessis. 1980. New Optical Technique for Measuring Erythrocyte Deformability with the Ektacytometer. *Clin. Chem.* 26:1435–1442.
15. Stadnick, H., R. Onell, J.P. Acker, and J.L. Holovati. 2011. Eadie-Hofstee analysis of red blood cell deformability. *Clin. Hemorheol. Microcirc.* 47:229–39.
16. Baskurt, O.K., M.R. Hardeman, M. Uyuklu, P. Ulker, M. Cengiz, N. Nemeth, S. Shin, T. Alexy, and H.J. Meiselman. 2009. Parameterization of red blood cell elongation index - Shear stress curves obtained by ektacytometry. *Scand. J. Clin. Lab. Invest.* 69:777–788.
17. Goldsmith, H.L., and J. Marlow. 1972. Flow behaviour of erythrocytes - I. Rotation and

- deformation in dilute suspensions. *Proc. R. Soc. London. Ser. B. Biol. Sci.* 182:351–384.
18. Parpart, A.K., and P.B. Lorenz. 1947. The osmotic resistance (fragility) of human red cells. *J. Clin. Invest.* 26:636–40.
 19. Tomaselli, M.B., K.M. John, and S.E. Lux. 1981. Elliptical erythrocyte membrane skeletons and heat-sensitive spectrin in hereditary elliptocytosis. *Proc. Natl. Acad. Sci. U. S. A.* 78:1911–5.
 20. Bessis, M. 1977. *Blood Smears Reinterpreted*. Berlin, Heidelberg: Springer Berlin Heidelberg.
 21. Discher, D.E., N. Mohandas, and E.A. Evans. 1994. Molecular maps of red cell deformation: hidden elasticity and in situ connectivity. *Science.* 266:1032–5.
 22. Robledo, R.F., S.L. Ciciotte, B. Gwynn, K.E. Sahr, D.M. Gilligan, N. Mohandas, and L.L. Peters. 2008. Targeted deletion of alpha-adducin results in absent beta- and gamma-adducin, compensated hemolytic anemia, and lethal hydrocephalus in mice. *Blood.* 112:4298–307.
 23. Discher, D.E., and N. Mohandas. 1996. Kinematics of red cell aspiration by fluorescence-imaged microdeformation. *Biophys. J.* 71:1680–94.
 24. Schneider, C.A., W.S. Rasband, and K.W. Eliceiri. 2012. NIH Image to ImageJ: 25 years of image analysis. *Nat. Methods.* 9:671–675.
 25. Raabe, B.M., J.E. Artwohl, J.E. Purcell, J. Lovaglio, and J.D. Fortman. 2011. Effects of weekly blood collection in C57BL/6 mice. *J. Am. Assoc. Lab. Anim. Sci.* 50:680–685.
 26. Gallagher, P.G. 2005. Red cell membrane disorders. *Hematology Am. Soc. Hematol. Educ. Program.* 13–18.
 27. Katnik, C., and R. Waugh. 1990. Electric fields induce reversible changes in the surface to volume ratio of micropipette-aspirated erythrocytes. *Biophys. J.* 57:865–75.
 28. Katnik, C., and R. Waugh. 1990. Alterations of the apparent area expansivity modulus of red blood cell membrane by electric fields. *Biophys. J.* 57:877–82.
 29. Danon, D. 1963. A rapid micro method for recording red cell osmotic fragility by continuous decrease of salt concentration. *J. Clin. Pathol.* 16:377–82.
 30. Nagasawa, T., S. Kojima, and E. Kimura. 1982. Coil planet centrifugal and capillary tube centrifugal analysis of factors regulating erythrocyte osmotic fragility and deformability. *Jpn. J. Physiol.* 32:25–33.
 31. Ungewickell, E., and W. Gratzer. 1978. Self-Association of Human Spectrin. A Thermodynamic and Kinetic Study. *Eur. J. Biochem.* 88:379–385.
 32. Bessis, M., and N. Mohandas. 1975. Red Cell Structure, Shapes and Deformability. *Br. J. Haematol.* 31:5–10.
 33. Dupire, J., M. Socol, and A. Viallat. 2012. Full dynamics of a red blood cell in shear flow. *Proc. Natl. Acad. Sci. U. S. A.* 109:20808–20813.
 34. Simmonds, M.J., and H.J. Meiselman. 2016. Prediction of the level and duration of shear stress exposure that induces subhemolytic damage to erythrocytes. *Biorheology.* 53:237–249.

35. Discher, D.E., D.H. Boal, and S.K. Boey. 1998. Simulations of the erythrocyte cytoskeleton at large deformation. II. Micropipette aspiration. *Biophys. J.* 75:1584–97.
36. Chilcote, R., M. Le Beau, C. Dampier, E. Pergament, Y. Verlinsky, N. Mohandas, H. Frischer, and J. Rowley. 1987. Association of red cell spherocytosis with deletion of the short arm of chromosome 8. *Blood.* 69:156–159.
37. Coetzer, T., and S. Zail. 1982. Spectrin tetramer-dimer equilibrium in hereditary elliptocytosis. *Blood.* 59:900–5.
38. Eber, S., and S.E. Lux. 2004. Hereditary spherocytosis—defects in proteins that connect the membrane skeleton to the lipid bilayer. *Semin. Hematol.* 41:118–141.
39. Liu, S.C., J. Palek, J. Prchal, and R.P. Castleberry. 1981. Altered spectrin dimer-dimer association and instability of erythrocyte membrane skeletons in hereditary pyropoikilocytosis. *J. Clin. Invest.* 68:597–605.
40. Zarkowsky, H.S., N. Mohandas, C.B. Speaker, and S.B. Shohet. 1975. A Congenital Haemolytic Anaemia with Thermal Sensitivity of the Erythrocyte Membrane. *Br. J. Haematol.* 29:537–543.
41. Chasis, J. a, P. Agre, and N. Mohandas. 1988. Decreased membrane mechanical stability and in vivo loss of surface area reflect spectrin deficiencies in hereditary spherocytosis. *J. Clin. Invest.* 82:617–23.
42. Cynober, T., N. Mohandas, and G. Tchernia. 1996. Red cell abnormalities in hereditary spherocytosis: Relevance to diagnosis and understanding of the variable expression of clinical severity. *J. Lab. Clin. Med.* 128:259–269.
43. Renoux, C., M. Faivre, A. Bessaa, L. Da Costa, P. Joly, A. Gauthier, and P. Connes. 2019. Impact of surface-area-to-volume ratio, internal viscosity and membrane viscoelasticity on red blood cell deformability measured in isotonic condition. *Sci. Rep.* 9:1–7.
44. Abkarian, M., M. Faivre, and A. Viallat. 2007. Swinging of Red Blood Cells under Shear Flow. *Phys. Rev. Lett.* 98:188302.
45. Skotheim, J.M., and T.W. Secomb. 2008. Red blood cells and other non-spherical capsules in shear flow: oscillatory dynamics and the tank-treading-to-tumbling transition. 1–11.
46. Sui, Y., H.T. Low, Y.T. Chew, and P. Roy. 2008. Tank-treading, swinging, and tumbling of liquid-filled elastic capsules in shear flow. *Phys. Rev. E - Stat. Nonlinear, Soft Matter Phys.* 77:1–10.
47. Boal, D. 2002. *Mechanics of the Cell.* 1st ed. Cambridge University Press.
48. Hansen, J.C., R. Skalak, S. Chien, and a Hoger. 1997. Influence of network topology on the elasticity of the red blood cell membrane skeleton. *Biophys. J.* 72:2369–81.
49. Begg, G.E., M.B. Morris, and G.B. Ralston. 1997. Comparison of the salt-dependent self-association of brain and erythroid spectrin. *Biochemistry.* 36:6977–6985.
50. Harris, A.S., L.A. David Green, K.J. Ainger, and J.S. Morrow. 1985. Mechanism of cytoskeletal regulation (I): functional differences correlate with antigenic dissimilarity in human brain and erythrocyte spectrin. *Biochim. Biophys. Acta - Protein Struct. Mol.*

Enzymol. 830:147–158.

51. Fai, T.G., A. Leo-Macias, D.L. Stokes, and C.S. Peskin. 2017. Image-based model of the spectrin cytoskeleton for red blood cell simulation. *PLOS Comput. Biol.* 13:e1005790.
52. Li, H., J. Yang, T.T. Chu, R. Naidu, L. Lu, R. Chandramohanadas, M. Dao, and G.E. Karniadakis. 2018. Cytoskeleton Remodeling Induces Membrane Stiffness and Stability Changes of Maturing Reticulocytes. *Biophys. J.* 114:2014–2023.
53. He, X., and J. Zhang. 2005. Rapid subfunctionalization accompanied by prolonged and substantial neofunctionalization in duplicate gene evolution. *Genetics.* 169:1157–1164.
54. Holland, P.W.H., F. Marlétaz, I. Maeso, T.L. Dunwell, and J. Paps. 2017. New genes from old: Asymmetric divergence of gene duplicates and the evolution of development. *Philos. Trans. R. Soc. B Biol. Sci.* 372.

Figure 1. Development and initial analysis of the α II β I mouse model. (A) Partial domain structures of spectrin in WT and α II β I knock-in mouse showing self-association sites and the location of the substituted α II repeats. (Upper) WT spectrin with α I-spectrin on the left (blue) and β I-spectrin on the right (yellow). The interaction of α - with β -spectrin occurs between α -R0 and β I-R17. (Lower) α II β I knock-in mouse spectrin: red indicates α -spectrin R0 and R1 from α II and R2-R4, in blue, from α I spectrin. β I-spectrin is unchanged in this mouse model. (B) Brightfield microscopy of red blood cells from WT and α II β I mice imaged using a Soret band-pass filter (413nm, 10nm) Scale bar = 20 μ m. (C) Analysis of the oligomerization state of spectrin in each mouse strain. Spectrin was extracted in low ionic strength medium at low temperature from erythrocytes from each mouse strain. The extracts were separated by non-denaturing gel electrophoresis and stained with Coomassie. The positions of spectrin dimers (D), tetramers (T) and higher oligomers (O) are indicated. (D) Increasing concentrations of α II-peptide resealed into RBC ghosts from WT and α II β I mice. (T) tetramer (D+P) dimer-peptide complex (D) dimer.

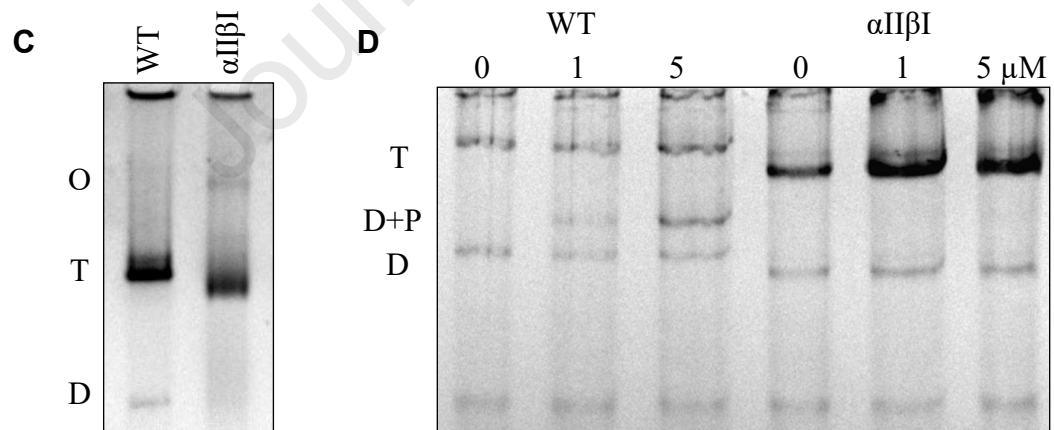
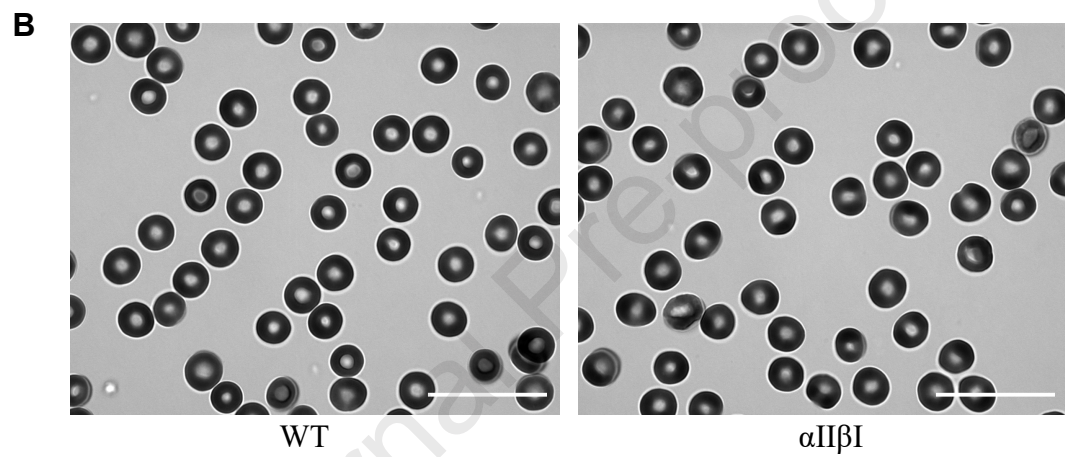
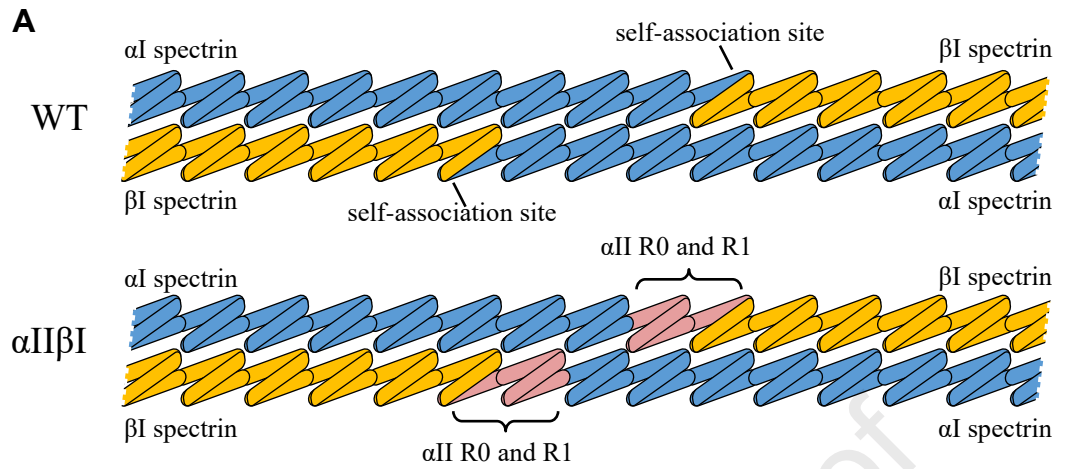
Figure 2. Effect of modified α II β I on membrane stability. (A) Surface area measured geometrically by micropipette aspiration. WT mean surface area $111.5 \pm 6.2 \mu\text{m}^2$ (n=53 cells) and α II β I $102.2 \pm 7.6 \mu\text{m}^2$ (n=44 cells), ~ 8.3% loss of surface area. (B) Osmotic fragility curves of WT (n=12 mice) and α II β I (n=5 mice) RBCs, error bars represent the SD and * $P \leq 0.05$, ** $P \leq 0.01$, *** $P \leq 0.001$ by unpaired student t-test.

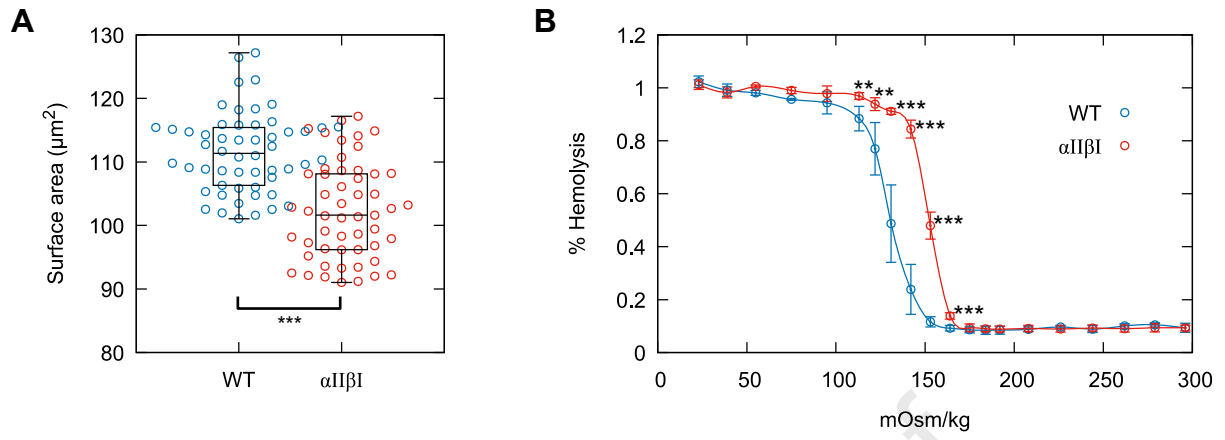
Figure 3. Thermal stability of red blood cells from WT and α II β I mouse. (A) The fraction of heat-induced spherical erythrocytes as at various temperatures from 45-50 $^{\circ}\text{C}$. Dashed lines showing the temperature at which 50% of red blood cells are spherical. * $P \leq 0.05$, ** $P \leq 0.01$, *** $P \leq 0.001$ by unpaired student t-test. (B) Brightfield microscopy of red blood cells from WT and α II β I mice imaged using a Soret band-pass filter (413nm, 10nm) after heating erythrocytes. Scale bar = 20 μ m.

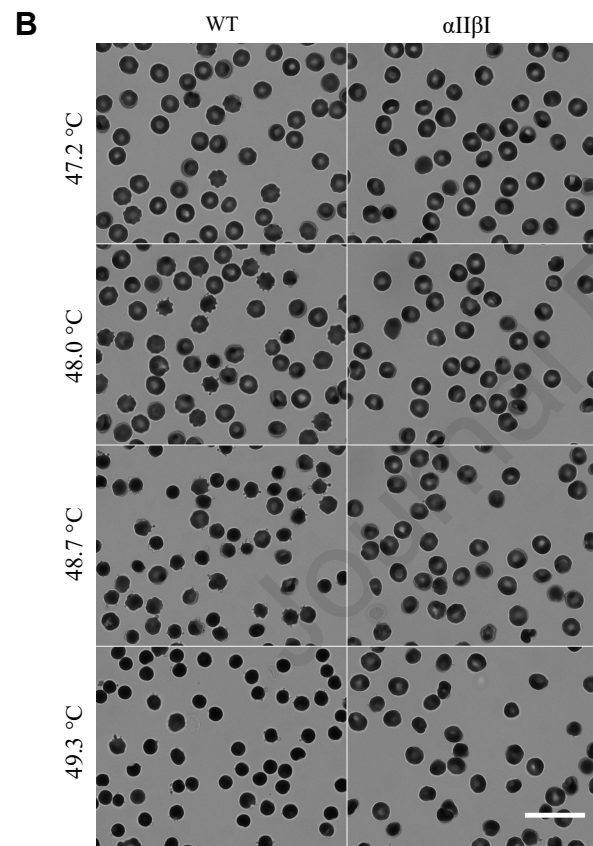
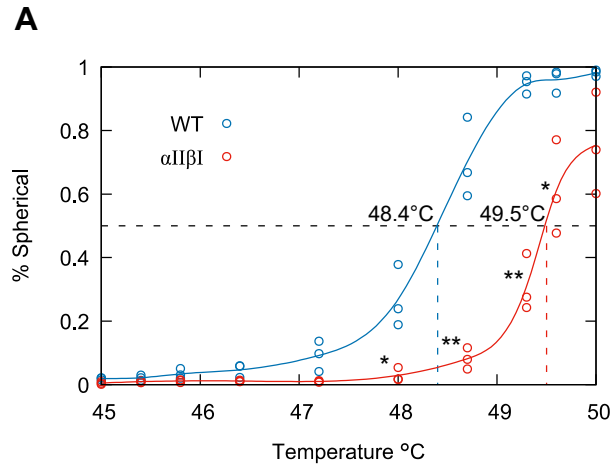
Figure 4. The deformability of WT and α II β I mouse red blood cells as a function of shear stress as measured by ektacytometry. WT sample is shown in blue and the α II β I shown in red. (A) The deformation index (DI) as a function of shear stress. (B) Eadie-Hofstee transformation of the ektacytometry data in A, the deformation index (DI) as a function of DI/(shear stress). (C) Rheoscope images of WT and α II β I red blood cells subject to increasing shear stress. Scale bar = 20 μ m.

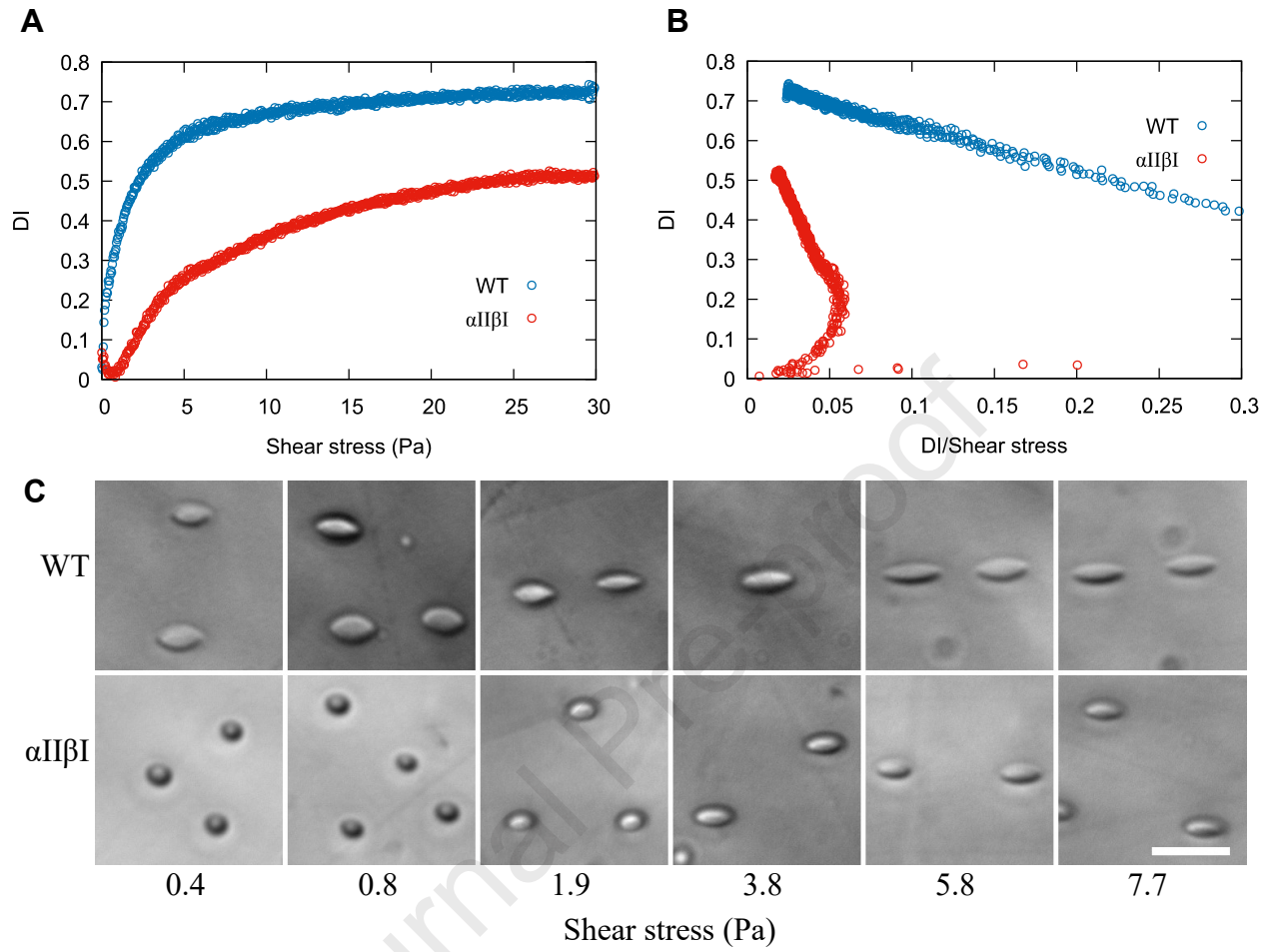
Figure 5. Fluorescence-imaged micro-deformation (A) Illustration of the aspirated red blood cell the red cell membrane indicated by the red line and the grey the micropipette. R_s , radius of spherical portion of cell outside micropipette; L , the length of aspirated portion of red cell; ρ_e , the fluorescent intensity at pipette entrance; ρ_c , the fluorescent intensity at cap of aspirated portion; R_p the internal radius of the micropipette. (B) The ratio of ρ_e and ρ_c of Band 3 in WT (blue) (n=8 cells) and α II β I (red) (n=14 cells) as a function of the normalized aspiration length L/R_p .

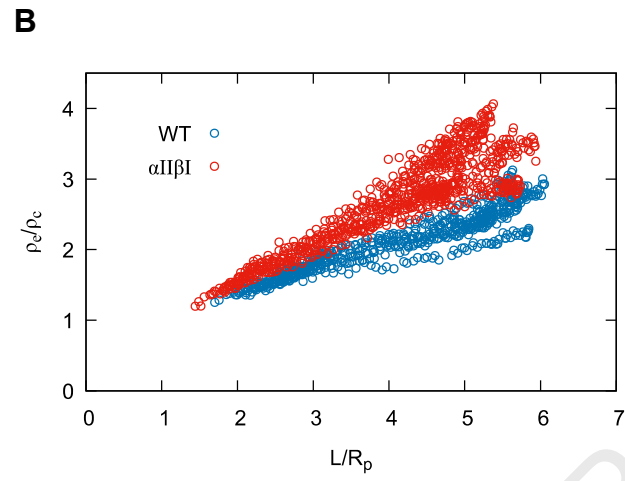
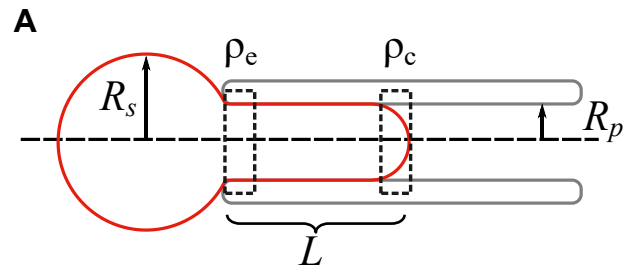
Figure 6. Fluorescence-imaged micro-deformation (A) ρ_e and ρ_c as a function of the normalized aspiration length L/R_p for aspirated red cells from both WT (blue) (n=8 cells) and α II β I (red) (n=14 cells) mice. (B) The computed principle components of membrane skeleton deformation as a function L/R_p for a cell with an aspiration length $L=6$. Inserts show the change in shape of a unit area of membrane skeleton, for the entrance of the micropipette (left) and the cap (right).

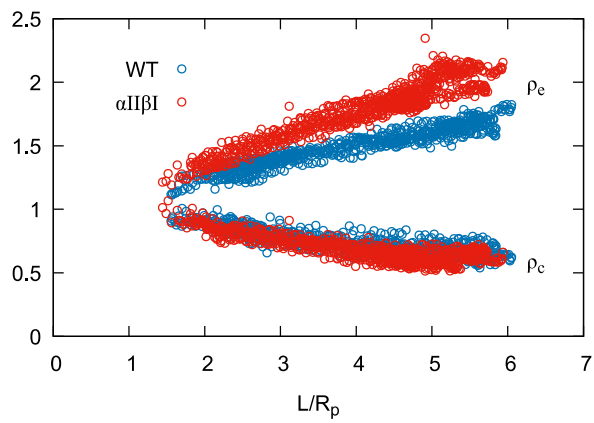










A**B**